Photoreflectance studies of optical transitions in type II $(GaAs)_m(AlAs)_n$ superlattices

2003 J. Phys.: Condens. Matter 15 3343

(http://iopscience.iop.org/0953-8984/15/19/333)

INSTITUTE OF PHYSICS PUBLISHING JOURNAL OF PHYSICS: CONDENSED MATTER

J. Phys.: Condens. Matter **15** (2003) 3343–3354 PII: S0953-8984(03)54659-8

Photoreflectance studies of optical transitions in type II $(GaAs)_m(AlAs)_n$ superlattices

G Wang[1], P Tronc[1], Yu E Kitaev[1,3] and R Planel[2,4]

[1] Ecole Supérieure de Physique et Chimie Industrielles, Laboratoire d'Optique Physique, 10 rue Vauquelin, 75231 Paris Cedex 05, France
[2] Laboratoire de Microstructures et Microélectronique, 196 Avenue H Ravera, 92260 Bagneux Cédex, France

E-mail: tronc@optique.espci.fr

Received 11 October 2002
Published 6 May 2003
Online at stacks.iop.org/JPhysCM/15/3343

Abstract

Photoreflectance (PR) spectra of two type II [001]$(GaAs)_m(AlAs)_n$ superlattices (SLs) have been measured at 77 K. In the conventional picture of the envelope-function approximation, the lowest conduction state originates, in the first sample, from the X_z point of the AlAs Brillouin zone (z being the growth direction) whereas it originates from the $X_{x,y}$ point in the second sample. Our spectra exhibit Franz–Keldysh oscillation (FKO) features and interband transition lines. The origin of the built-in electric field within the samples is discussed and its strength calculated from FKOs. For interpreting our spectra of interband optical transitions, a least-squares fit of the data to the Aspnes third-derivative functional form has been performed as well as computation of the optical transition energies. From the energy and amplitude of the interband transition lines in PR spectra, we showed that the two SLs are pseudo-direct, i.e. the ground optical transition in any of them is direct in the k space and takes place at the Γ point of the SL Brillouin zone. All the other interband transitions appearing in the SL spectra are also direct in k space.

1. Introduction

The space groups of the [001]$(GaAs)_m(AlAs)_n$ superlattices (SLs) have been shown [1] to be D^5_{2d} for even values of $m+n$ and D^9_{2d} for odd values. We previously studied these SLs from the point of view of symmetry and established the optical selection rules at the symmetry points of the SL Brillouin zone (SLBZ), for both direct transitions and phonon-assisted ones [1, 2]. In addition to the Γ point of SLBZ, the Z point of the SLs with the D^5_{2d} space group and the

[3] Permanent address: AF Ioffe Physico-Technical Institute, Politekhnicheskaya 26, 194021 St Petersburg, Russia.
[4] Deceased.

M point of the SLs with the D^9_{2d} space group are of particular interest for our study since they are located at the surface of the SLBZ in a direction parallel to the growth axis [1]. Within the envelope-function approximation (EFA), the [001](GaAs)$_m$(AlAs)$_n$ SLs can be either of type I (the ground transition takes place between holes and electrons both confined in GaAs layers) or of type II (the ground transition takes place between holes in GaAs layers and electrons in AlAs layers). The type depends on the thicknesses of the GaAs and AlAs slabs [3]. Moreover, the electrons involved in the ground transition of the type II SLs may originate either from the X_z point of the AlAs Brillouin zone (BZ) or from the $X_{x,y}$ point, depending also on layer thicknesses [3].

The electron structure and optical properties of both type I and type II (GaAs)$_m$(AlAs)$_n$ SLs grown along the [001] direction have been extensively studied experimentally. A variety of optical techniques have been used for the experimental studies, such as for example absorption [4], photoluminescence (PL) [3, 5–7], photoluminescence excitation (PLE) [5, 6], photocurrent [8–10] and optically detected magnetic resonance [11] spectroscopy. These methods provide valuable information about the band structure of the samples under consideration. However, there are often some limiting conditions for using them. For example, PL and PLE experiments are in most of the cases performed at low temperatures to provide more detailed information. On the other hand, absorption spectroscopy experiments can be performed at room temperature, but in some cases, a window must be etched in the substrate to allow a sufficient amount of light to be detected, which generally induces strain in the structure.

The modulation technique of photoreflectance (PR) has been proven to be a simple, contactless and sensitive probe of interband transitions in bulk materials [12] and in quantum wells (QWs), even at room temperature [13, 14]. Nevertheless it has not been yet used to a great extent in SL research. This may be at least partially due to the fact that the structure of SLs and their electron properties are much more complicated than those of bulk materials and QWs.

In this paper, we report on the use of the PR spectroscopy to study interband transitions in two type II [001](GaAs)$_m$(AlAs)$_n$ SLs at 77 K.

2. Samples and experiment

2.1. Samples

The two samples used in our PR experiments are type II (GaAs)$_m$(AlAs)$_n$ SLs grown by molecular beam epitaxy on [001] GaAs substrates and characterized by x-ray diffraction. Their structure is presented in figure 1. Sample I is composed of 80 periods of GaAs (13.8 Å)–AlAs (28.07 Å) slabs ($m = 5, n = 10$). The cap layer (CP) is made of undoped GaAs (60 Å). The buffer layers are made of undoped AlAs (1000 Å) and GaAs (5000 Å). The GaAs substrate is n doped (10^{18} cm^{-3}). The lowest-energy electron state originates [3, 4] from the X_z state of AlAs. Sample II is composed of 80 periods of GaAs (24.04 Å)–AlAs (96.16 Å) slabs ($m = 8, n = 34$). The CP is made of undoped GaAs (280 Å) and the buffer layer of undoped GaAs (5000 Å). The GaAs substrate is n doped (10^{18} cm^{-3}). The lowest energy electron state originates [3, 4] from the $X_{x,y}$ state of AlAs.

The SL of sample I has the D^9_{2d} space symmetry and the SL of sample II the D^5_{2d} one. Local fluctuations of the slab thicknesses generally occur in the growth process of QWs and SLs. Except for the case of ultrathin slabs, the symmetry properties [1, 2] of SLs do not dramatically depend on the parity of $m+n$. Moreover, any symmetry property which will be used hereafter does not depend on it [1, 2].

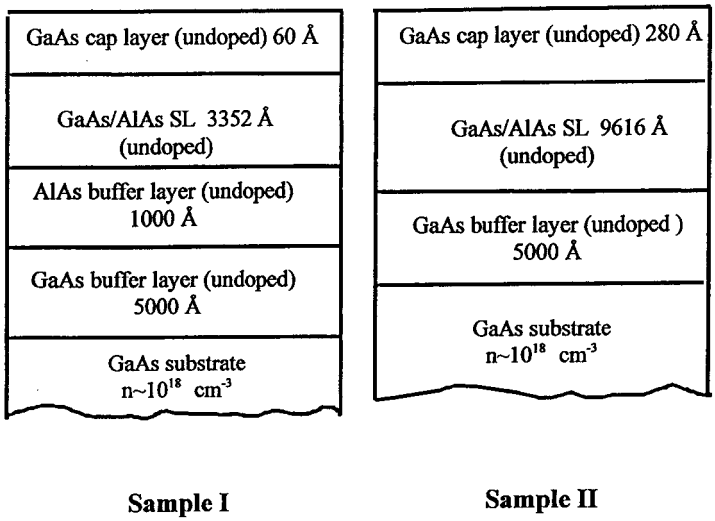

Figure 1. Structure of samples I and II.

2.2. Experimental set-up

The experimental arrangement used to measure PR spectra is shown elsewhere [15]. Light from a halogen lamp (100 W) passing through an HR320 Jobin Yvon monochromator was used as a probe beam with small-angle incidence. The pump beam was the 5320 Å green line of a doubled YAG laser chopped at 14 Hz. The two beams were focused onto the same spot on the sample, the size of the probe beam on the sample being 4 mm × 1 mm and the power density of the pump beam 0.021 W cm^{-2}.

The reflected probe beam was detected with the help of a photomultiplier. An OG570 Schott filter was used in front of the detector in order to prevent the laser beam reaching the detector and a lens with a great focal length to avoid the luminescence light appearing in the spectra.

The measurements were performed at 77 K, the time constant of the lock-in amplifier being 3 s.

3. Results

Figures 2 and 3 display the PR spectra (dotted curves) of samples I and II respectively in the 1.4–2.2 eV energy range. Each spectrum was obtained by recording the signal 20 times without changing any experimental condition. The solid curves in both spectra are a least-squares fit of the data using the Aspnes third-derivative functional form (TDFF) expression [16]:

$$\frac{\Delta R}{R} = \sum_{j}^{m} \mathrm{Re}[C_j e^{i\theta_j}((E - E_j) + i\Gamma_j)^{n_j}] \tag{1}$$

where m is the total number of spectral features in the region to be fitted, C_j, θ_j, E_j and Γ_j are the amplitude, phase, energy, and broadening parameters, respectively, of the jth structure, and n_j depends on the dimensionality of the structure. The value of n is -3 and -2.5 for two- and three-dimensional structures respectively.

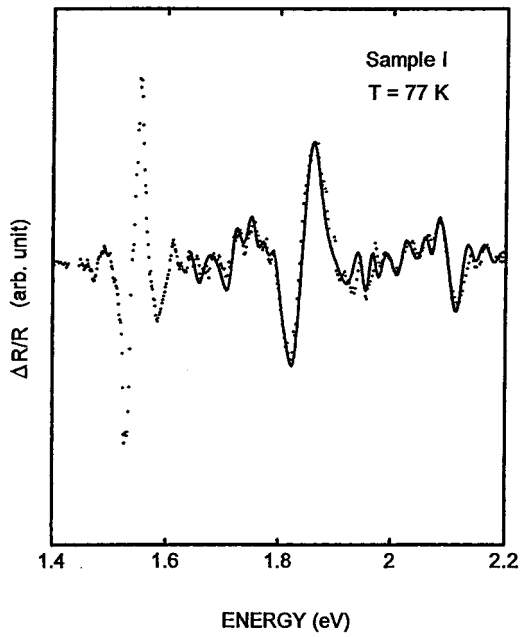

Figure 2. PR spectrum of sample I recorded at 77 K (dotted curve). The fit to the data is shown as a solid curve.

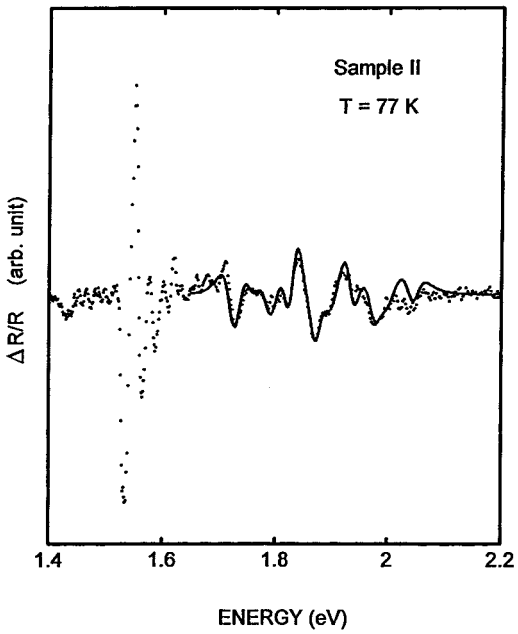

Figure 3. PR spectrum of sample II recorded at 77 K (dotted curve). The fit to the data is shown as a solid curve.

3.1. Franz–Keldysh oscillations

It is well known that, for a semiconductor in an electric field, the oscillatory behaviour of PR spectra at $E > E_g$, where E is the photon energy and E_g the bandgap energy respectively, can

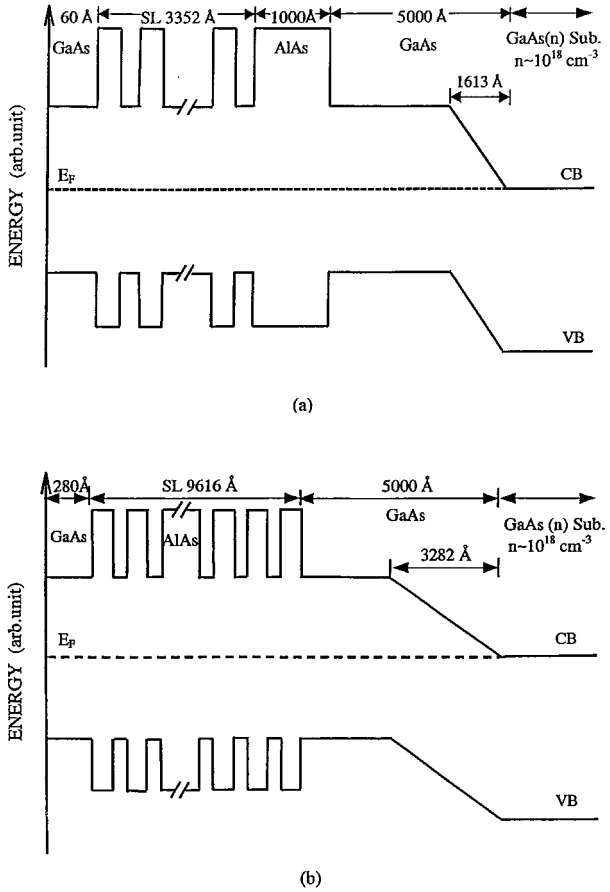

Figure 4. Conduction band (CB) and valence band (VB) edge profile in (a): sample I; (b) sample II.

be described by an electro-optic function, whose asymptotic form [17] can be written as:

$$\Delta R/R \sim \cos\{(4/3)[(E - E_g)/(\eta\theta)]^{3/2} + \pi(\delta - 1)/2\} \tag{2}$$

where $(\eta\theta)^3 = e^2\eta^2F^2/2\mu$, δ is the dimensionality of the critical point [17], F is the electric field strength and μ ($\mu^{-1} = m_e^{-1} + m_h^{-1}$) the reduced interband effective mass in the direction of the electric field.

The extrema in Franz–Keldysh oscillations (FKOs) are given from equation (2) by

$$\nu\pi = \varphi + [(E_\nu - E_g)/\eta\theta]^{3/2} \tag{3}$$

where E_ν is the energy of the νth extremum and φ is a phase factor. A plot of $(E_\nu - E_g)^{3/2}$ versus ν yields a straight line whose slope is proportional to F.

Sample I. An electric field within the undoped GaAs buffer layer originates from alignment of the Fermi level in the buffer layer and in the doped substrate. The Fermi level lies at the bottom of the conduction band (CB) in a doped substrate (figure 4(a)), inducing a 0.76 V potential difference between the buffer and the substrate. The PR spectrum of sample I (figure 2) exhibits FKOs above the bandgap energy of GaAs due to the electric field which extends near the substrate in the GaAs buffer layer. Figure 5(a) exhibits the plot of $(E_\nu - E_g)^{3/2}$ versus ν.

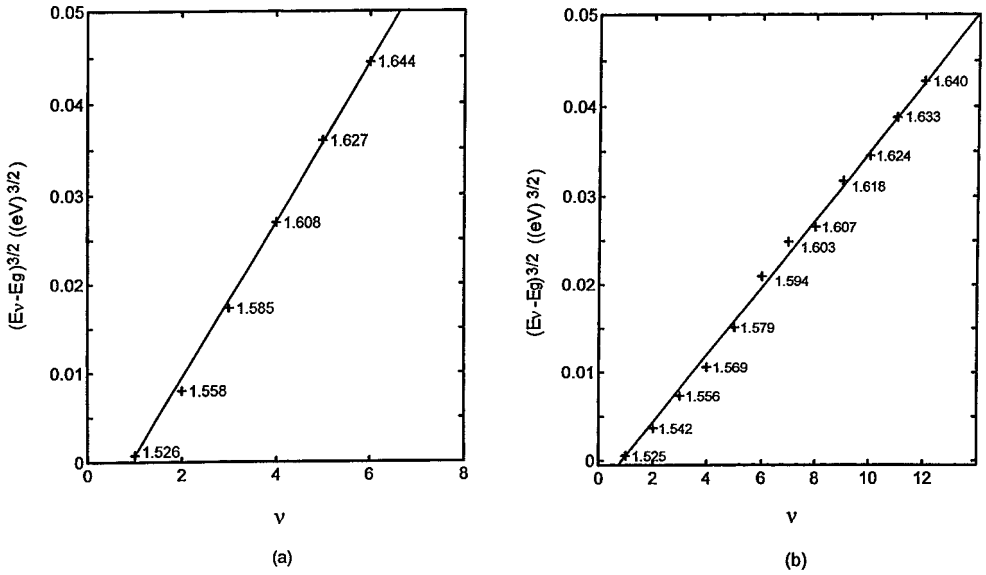

Figure 5. Plot of $(E_\upsilon - E_g)^{3/2}$ versus extremum index υ. The energy values (in eV) corresponding to each extremum in the FKOs region of the PR spectrum is indicated: (a) sample I; (b) sample II.

Table 1. Values at 77 K, along the [001] direction, of bandgap energy in eV and effective masses in unit of m_0 (mass of free electron). The subscripts t and l refer to transverse and longitudinal value respectively.

		GaAs	AlAs
Bandgap energy	$E_g(\Gamma)$	1.511	3.1
	$E_g(X)$	1.91	2.161
CB effective mass	$m_e(\Gamma)$	0.067	0.13
	$m_e(X_t)$	0.23	0.19
	$m_e(X_l)$	1.3	1.1
VB effective mass	m_{hh}	0.38	0.70
	m_{lh}	0.095	0.15

It can be seen that the six extrema lie along a straight line. Using a $0.06\,m_0$ reduced interband effective mass in GaAs provides an electric field strength F value of 46.8 kV cm^{-1} and an extension of the electric field in the GaAs buffer layer of 1613 Å (figure 4(a)).

Sample II. The situation is similar to that in sample I. The potential profile within the sample is shown in figure 4(b). The plot of $(E_\nu - E_g)^{3/2}$ versus ν (figure 5(b)) exhibits 12 extrema lying along a straight line and providing an electric field strength of 23 kV cm^{-1}. The extension of the electric field in the buffer layer is 3282 Å (figure 4(b)).

3.2. Interband optical transitions

For both samples, the interband optical transition energies have been computed using EFA. The built-in electric field which extends in the GaAs buffer layer does not penetrate into the SL and therefore does not affect its energy levels. The parameters used in calculations are taken from [18] and are listed in table 1. The band offset is taken to be equal to 0.67. The calculated

Table 2. Calculated SL miniband width in meV for heavy holes (HH), light holes (LH) and electrons confined in GaAs slabs (E^{Γ}) and in AlAs slabs ($E^{z(x,y)}$). In each column, the minibands are displayed according to increasing values of carrier energy.

Sample I				Sample II					
Hole		Electron		Hole		Electron			
HH_1	0.2	E_1^z	0.3	HH_1	0	E_1^{Γ}	0	E_6^z	0.1
HH_2	2.4	E_2^z	4	LH_1	13	E_1^z	0	E_7^z	0.2
LH_1	45	E_3^z	14			E_2^z	0	E_8^z	0.5
		$E_1^{x,y}$	17			E_3^z	0	$E_2^{x,y}$	0.9
		E_1^{Γ}	22			E_4^z	0	$E_3^{x,y}$	2.6
		$E_2^{x,y}$	72			E_5^z	0	$E_4^{x,y}$	6.5
						$E_1^{x,y}$	0.1		

Table 3. Energy, broadening parameter and amplitude of interband transitions obtained from the best fit of equation (3) for sample I. The calculated energy of transitions and the squared modulus of the overlap α of the electron and hole envelope functions are also given together with the values of the k_z wavevector of the electron and hole envelope functions within the Γ–M SL miniband.

	Energy (eV)		Broadening parameter	Relative		Wavevector k_z	
Spectral feature	Fit	Calc.	(meV)	amplitude	$\lvert\alpha\rvert^2$	Electron	Hole
GaAs		1.511					
e_1–lh_1 (CP)	1.659	1.657	22.9	0.05	0.9920		
E_1^z–hh_1 (SL–CP)	1.718	1.719	22.0	0.08	0.0024	$\pi/2d$	
E_1^z–lh_1 (SL–CP)	1.754	1.760	24.2	0.12	0.0051	$\pi/2d$	
e_1–hh_3 (CP)	1.770	1.771	25.2	0.13	0.8198		
E_2^z–hh_1 (SL–CP)	1.795	1.802	23.1	0.08	0.0043	$\pi/2d$	
E_2^z–lh_1 (SL–CP)	1.836	1.839	27.2	0.18	0.0072	$\pi/2d$	
E_1^z–HH_1 (SL)	1.850	1.854	35.6	1.00	0.3154	0	0
E_2^z–HH_1 (SL)	1.932	1.934	28.1	0.32	0.2563	π/d	π/d
E_3^z–lh_1 (SL–CP)	1.955	1.958	25.6	0.20	0.0150	$\pi/2d$	
E_2^{xy}–hh_2 (SL–CP)	1.975	1.972	24.2	0.09	0.0287	$\pi/2d$	
E_2^z–lh_2 (SL–CP)	2.018	2.017	25.1	0.08	0.0089	$\pi/2d$	
e_1–hh_5 (CP)	2.065	2.070	24.1	0.13	0.1436		
E_3^z–hh_3 (SL–CP)	2.076	2.072	25.3	0.17	0.0185	$\pi/2d$	
E_2^z–LH_1 (SL)	2.116	2.110	27.4	0.17	0.4890	π/d	π/d
E_1^{Γ}–HH_1 (SL)	2.150	2.146	22.5	0.03	0.9415	0	0
E_3^z–LH_1 (SL)	2.181	2.182	23.1	0.02	0.3390	0	0

miniband widths in both samples are listed in table 2. The calculated energies of the interband transitions appearing in PR spectra, together with the parameters provided by the best fit of spectra using equation (1), are displayed in table 3 for sample I and in table 4 for sample II. In the tables, the labels HH (hh) and LH (lh) refer to heavy- and light-hole states respectively, which are confined in SL (CP) GaAs slabs. The label e refers to electron states confined in CP whereas E^{Γ} refers to electron states confined in SL GaAs slabs and E^z and $E^{x,y}$ refer to the states confined in SL AlAs slabs. The E_z and E_{xy} states originate from the X_z and $X_{x,y}$ electron states respectively in bulk AlAs. The C amplitude of the lines in PR spectra (see formula (1)) has been normalized by setting the amplitude of the most intense line in every SL (E_1^z–HH_1 in SL of sample I and $E_1^{x,y}$–LH_1 in SL of sample II) equal to 1. Tables 3 and 4 also provide the squared modulus of the calculated overlap α of electron and hole envelope functions as well as the values of the envelope-function wavevector k_z along the z direction of both the electrons

Table 4. Energy, broadening parameter, and amplitude of interband transitions obtained from the best fit of equation (3) for sample II. The calculated energy of transitions and the squared modulus of the overlap α of the electron and hole envelope functions are also given together with the values of the k_z wavevector of the electron and hole envelope functions within the Γ–Z SL miniband.

	Energy (eV)		Broadening parameter	Relative		Wavevector k_z	
Spectral feature	Fit	Calc.	(meV)	amplitude	$\|\alpha\|^2$	Electron	Hole
GaAs		1.511					
E_1^{xy}–HH_1 (SL)	1.748	1.744	32.6	0.99	0.072	0	0
E_1^{z}–HH_1 (SL)	1.758	1.755	34.1	0.29	0.065	0	0
E_3^{z}–HH_1 (SL)	1.792	1.781	31.2	0.31	0.015	0	0
E_3^{xy}–HH_1 (SL)	1.831	1.832	24.3	0.40	0.016	0	0
E_1^{xy}–LH_1 (SL)	1.853	1.854	33.0	1.00	0.040	0	0
E_1^{z}–LH_1 (SL)	1.865	1.865	27.2	0.35	0.025	0	0
E_1^{Γ}–HH_1 (SL)	1.875	1.878	28.5	0.54	0.735	0	0
E_3^{z}–LH_1 (SL)	1.890	1.890	35.4	0.70	0.089	0	0
E_7^{z}–HH_1 (SL)	1.906	1.906	36.5	0.67	0.051	0	0
E_3^{xy}–LH_1 (SL)	1.936	1.940	26.8	0.42	0.065	0	0
E_1^{Γ}–LH_1 (SL)	1.985	1.987	30.5	0.50	0.105	0	0
E_9^{z}–HH_1 (SL)	2.001	2.003	34.0	0.41	0.053	0	0
E_7^{z}–LH_1 (SL)	2.018	2.016	27.9	0.22	0.084	0	0
E_8^{z}–LH_1 (SL)	2.045	2.062	29.1	0.19	0.007	π/d	π/d

and the holes within the SL miniband (d is the SL period along the z direction). The k_z values appearing in tables 3 and 4 correspond to the maximal value of $|\alpha|$ in the SL miniband for each transition taking place within the SL or at the SL–CP interface (for the latter transitions, the minimal values of $|\alpha|$ always occur at the ends of the Γ–$Z(M)$ conduction miniband, i.e. for k_z equal to 0 or to π/d respectively, whereas the maximal value of $|\alpha|$ occurs at the middle of the miniband, i.e. for k_z equal to $\pi/2d$. A typical example is given in figure 6). The indices of electron and hole states in the tables correspond to the best fit between each measured transition energy and the computed one. Our experiments were performed at approximately 77 K. The corresponding kT energy value is 7 meV. We assume that excitonic features are absent in our measurements. Indeed, an indirect exciton in the SL, i.e. an exciton made of a hole and an electron confined in GaAs and AlAs SL slabs, respectively, has a binding energy smaller than that of an exciton in bulk GaAs (4.6 meV) and should be dissociated at the temperature of our experiments. This also holds for an exciton made of a hole (electron) confined in the CP and an electron (hole) in the SL. Finally, let us consider the recombination of an electron and a hole both confined within the CP (the e_1–lh_1, e_1–hh_3, and e_1–hh_5 transitions in sample I, see table 3) or within the SL GaAs slabs (the E_1^{Γ}–HH_1 transition in sample I, see table 3, and the E_1^{Γ}–HH_1 and E_1^{Γ}–LH_1 transitions in sample II, see table 4). Direct excitons obviously can have a larger binding energy than the indirect ones mentioned above. Nevertheless, the best agreement with measurements is obtained when assuming no exciton formation, i.e. without subtracting any binding energy from the computed band-to-band transition energy (except perhaps for the e_1–hh_5 transition in sample I). This supports our assumption about the absence of excitons.

The transitions listed in the CP and in the SL (tables 3 and 4) are all allowed from parity with respect to z. As a matter of fact, using a tight-binding approximation and considering direct optical transitions in the (x, y) polarization, it has been shown [19] in EFA that a type I allowed (forbidden) transition at the Γ point of SLBZ is also allowed (forbidden) at the $Z(M)$ point of SLBZ in the same miniband. On the contrary, for a type II transition with an electron arising from the X_z or $X_{x,y}$ point of bulk AlAs, the characters are opposite at each end of the

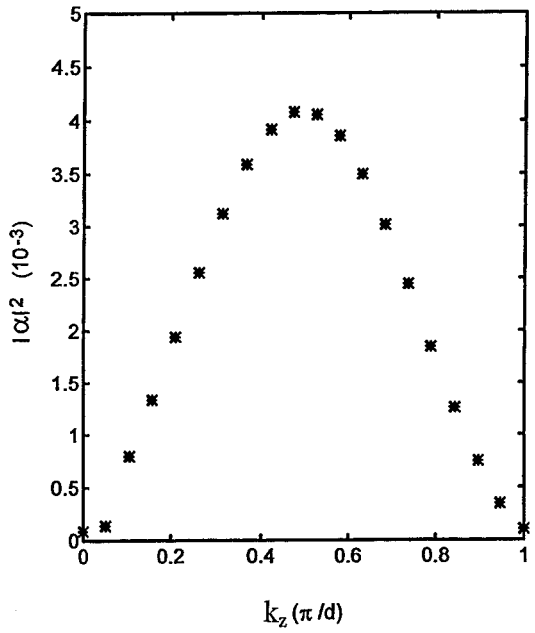

Figure 6. Squared modulus of the overlap α of electron and hole envelope functions versus the electron wavevector k_z for the E_1^z–lh_1 transition at the SL–CP interface in sample I.

miniband. The result arises from the spatial configuration of the electron and hole envelope functions [19] (the parity with respect to z of an envelope function is the same at the Γ and $Z(M)$ points of SLBZ). Computation shows that, within any SL miniband, the energy of an electron (hole) varies monotonically versus the k_z vector modulus. In agreement with the prediction of [19], the E_2^z–LH_1 transition in the SL of sample I, which is forbidden from parity with respect to z at the Γ point, takes place at the M point of SLBZ (tables 2 and 3). For the E_2^z–HH_1 transition in sample I, the E_2^z and HH_1 minibands are too narrow (4 and 0.2 meV, respectively, cf table 2) to allow an accurate check of the prediction using the experimental results. The prediction of [19] also holds for the E_8^z–LH_1 transition in the SL of sample II (table 4). It takes place at the Z point of SLBZ. To summarize, it has thus to be concluded that any transition appearing in the PR spectra of each SL is direct in the SL k space. Of course, there are no selection rules for the transitions at the SL–CP interface since no translational periodicity is involved. Note that computation provides an energy of 1.616 eV for the e_1–hh_1 transition within the CP of sample I. The transition should therefore appear in the FKOs region but is masked by FKOs (figure 2). The CP of sample II, being very wide (280 Å), induces no appreciable confinement for carriers. The only lines appearing in the PR spectrum of sample II correspond to interband transitions within the SL (table 4). The absence of oblique transitions at the SL–CP interface of sample II probably arises from the small overlap of the electron and hole envelope functions. Indeed, the envelope functions in the CP are widely spread due to the large width of the CP, which makes the probability of presence near the interface very low.

4. Discussion

As shown above, the agreement between calculated and measured values of energy for any transition is satisfactory. For most of the transitions, the difference between the two values is

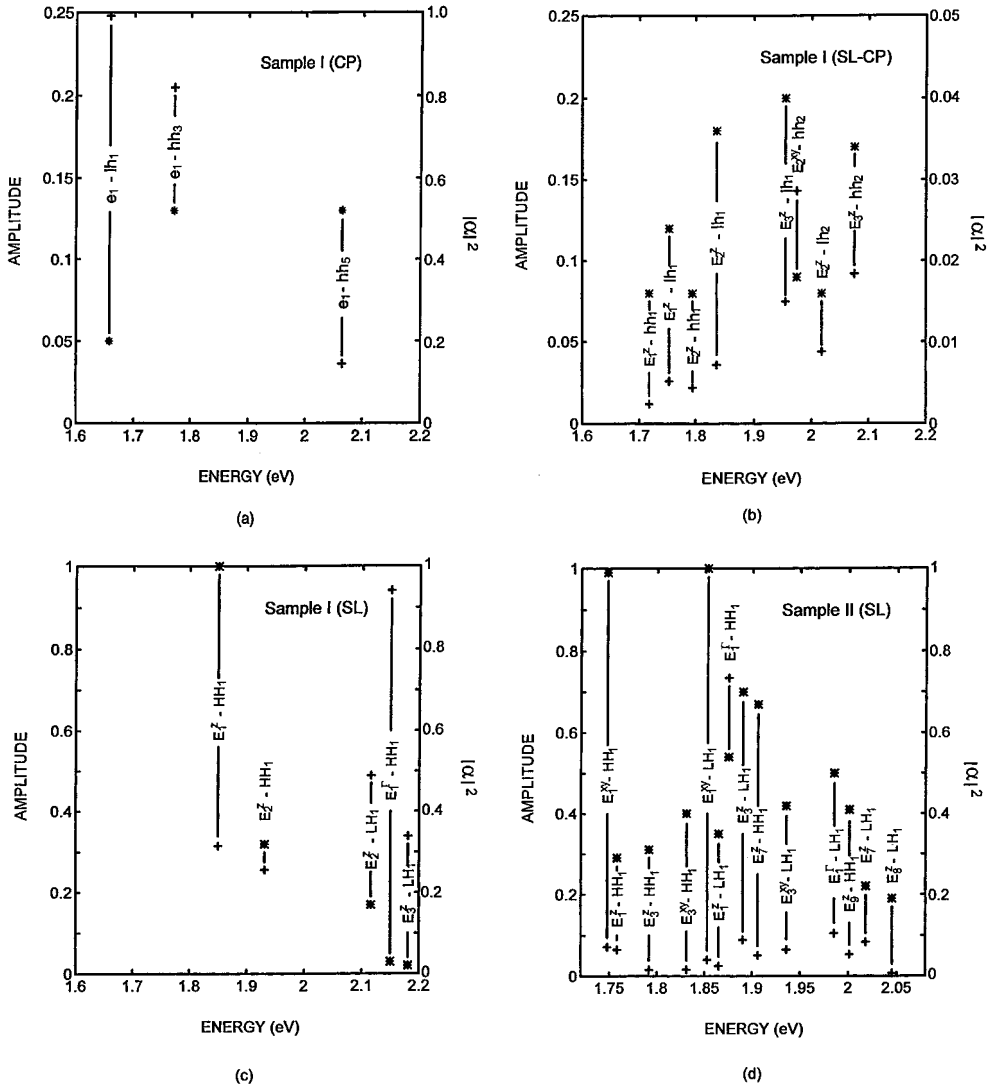

Figure 7. Amplitude C ($*$) and squared modulus of the overlap α of the electron and hole envelope functions (+) for transitions: (a) in CP of sample I; (b) at SL–CP interface of sample I; (c) in SL of sample I; (d) in SL of sample II.

less than 5 meV. Moreover, the variation of transition amplitude versus transition energy in the SLs as well as in the CP and at the SL–CP interface of sample I provides additional information about recombination processes in the samples. For this purpose, values of the amplitude C of the transitions in the fit to the Aspnes form and corresponding values of $|\alpha|^2$, all taken from tables 3 and 4, are plotted in figures 7(a)–(d) versus transition energy. It can be seen that the ratio $C/|\alpha|^2$ does not dramatically vary from one transition to another, either within the CP or at the SL–CP interface of sample I, whereas it decreases very rapidly when transition energy increases within the SL. In sample II, only transitions within the SL are present in the PR spectra, and the above ratio does not vary dramatically with energy.

The type II transitions, when allowed from symmetry, are expected of course to have an oscillator strength weaker than that of an allowed transition between an electron and a hole both confined in SL GaAs slabs (at least weaker than that of a transition in SL GaAs slabs between an electron and a hole with envelope functions having the same index). Indeed, the $|\alpha|$ value for type II transitions is smaller due to the confinement of electrons and holes in AlAs and GaAs slabs respectively. Besides, any phonon-assisted transition is allowed between the $Z(M)$ or any other symmetry point of SLBZ on one hand and the Γ point on the other hand, whatever the symmetries of both the initial and final states [1, 2]. Nevertheless, these transitions are expected to be very weak in our experiments since the intensity of such processes in general decreases dramatically in semiconductor structures with increasing temperature making them disappear before reaching 77 K. This allows us to conclude that the most intense transitions in the SL spectra, i.e. E_1^z–HH_1 in the SL of sample I, $E_1^{x,y}$–HH_1 and $E_1^{x,y}$–LH_1 in the SL of sample II, cannot be phonon-assisted. This is consistent with the results of computation of direct band-to-band transition energies (tables 3 and 4), which are in good agreement with the experimental data. From their amplitude, the same conclusion can be drawn about the nature (direct in the k space) of the E_2^z–HH_1, E_2^z–LH_1, and E_3^z–LH_1 transitions, also present at higher energies in the SL spectra of sample I. Indeed, the amplitudes of the lines decrease very rapidly with increasing transition energy (table 3, figure 7(c)), but it should be noticed that the E_1^Γ–HH_1 transition in the SL, which is expected to have a strong amplitude since it is direct in real space and fully allowed, is also actually weak. The decrease of amplitude with increasing transition energy is assigned to the numerous transitions at the SL–CP interface (transitions which are oblique in the real space). They have a fairly strong amplitude (table 3). The populations of excited states in the SL shrink rapidly since the CP offers broad channels for recombination. Indeed, E_1^z electrons in the SL partly recombine with hh_1 and lh_1 holes in the CP, as well as E_2^z with hh_1, lh_1 and lh_2, E_3^z with lh_1 and hh_3, and $E_2^{x,y}$ with hh_2. In the SL of sample I, for any conduction state confined in the AlAs slabs, the sum of the amplitudes of its oblique transitions to CP valence states increases with its energy (table 3, figure 7(b)). The oblique transitions from the E_3^z state are preponderant in amplitude when compared to those in the SL (table 3, figure 7(c)). For the $E_2^{x,y}$ states, no transition is detected within the SL. All the transitions appearing in the PR spectra of the SL of sample I are therefore direct in the SL k space. The E_1^z–HH_1, E_1^Γ–HH_1 and E_1^z–LH_1 transitions take place at the Γ point whereas the E_2^z–HH_1 transition and probably the E_2^z–LH_1 one take place at the M point. For the SL of sample II (table 4), in addition to the $E_1^{x,y}$–HH_1 and $E_1^{x,y}$–LH_1 transitions, which are the most intense ones, all other transitions ($E_3^{x,y}$–HH_1, $E_3^{x,y}$–LH_1, E_1^Z–HH_1, E_3^z–HH_1, E_1^z–LH_1, E_3^z–LH_1, E_7^z–HH_1, E_9^z–HH_1, E_7^z–LH_1 and E_8^z–LH_1) are also of type II and are of the same order of magnitude as the direct transitions at the Γ point of SLBZ (E_1^Γ–HH_1 and E_1^Γ–LH_1). Again, these results confirm the assignment of all the lines to direct transitions in the k space of SLBZ (at the Γ point for any transition, except for the E_8^z–LH_1 one which takes place at the Z point).

Finally, many transitions are missing in our spectra, such as for example the E_2^z–HH_2 one in the SL of sample I or any transition involving the $E_2^{x,y}$ states in the SL of sample II. It is likely that these transitions are present but not intense enough to appear clearly.

5. Conclusion

The study by PR spectroscopy of two type II $[001](GaAs)_m(AlAs)_n$ SLs allowed us to find evidence for numerous interband transitions within the SLs. The transitions are either direct in real space (electron and hole both confined in GaAs slabs) or oblique (electron and hole confined in GaAs and AlAs slabs respectively). All the transitions are direct in the SL k

space. Most of them take place at the Γ point of SLBZ, whereas a few others take place at the $Z(M)$ point. The results are in agreement with predictions from EFA. In this approach, a tight-binding representation of the Γ–$Z(M)$ minibands provides valuable predictions for the optical selection rules. In the sample with a thin CP (sample I), the high-energy conduction electrons confined within the SL preferentially recombine with the holes of the CP, whereas a thick CP (sample II) seems to offer no efficient channel for oblique recombination of electrons.

References

[1] Kitaev Yu E, Panfilov A G, Tronc P and Evarestov R A 1997 *J. Phys.: Condens. Matter* **9** 257
[2] Tronc P and Kitaev Yu E 2001 *Phys. Rev.* B **63** 205326
[3] Scalbert D, Cernogora J, Benoit à la Guillaume C, Maaref M, Charfi F F and Planel R 1989 *Solid State Commun.* **70** 945
[4] Violotis V, Grousson R, Lavallard P, Ivchenko E L, Kiselev A A and Planel R 1994 *Phys. Rev.* B **49** 2576
[5] Moore K J, Duggan G, Dawson P and Foxon C T 1988 *Phys. Rev.* B **38** 5535
[6] Danan G, Etienne B, Mollot F, Planel R, Jean-Louis A M, Alexandre F, Jusserand B, Le Roux G, Marzin J Y, Savary H and Sermage B 1987 *Phys. Rev.* B **35** 6207
[7] Meynadier M-H, Nahory R E, Worlock J M, Tamargo M C, de Miguel J L and Sturge M D 1988 *Phys. Rev. Lett.* **60** 1338
[8] Fujiwara K, Kawashima K, Yamamoto T, Sano N, Cingolani R, Grahn H T and Ploog K 1993 *Phys. Rev.* B **49** 1809
[9] Schwedler R, Brüggemann F, Kohl A, Wolter K, Leo K and Kurz H 1993 *Appl. Phys.* A **57** 199
[10] Schneider H, Fischer A and Ploog K 1991 *Phys. Rev.* B **45** 6329
[11] van Kesteren H W, Cosman E C, Dawson P, Moore K J and Foxon C T 1989 *Phys. Rev.* B **39** 13426
[12] Pollak F H 1981 *Proc. Conf. on Optical Characterization Techniques for Semiconductor Technology (The Society of Photo-Optical Instrumentation Engineers) (Bellington, Washington, 1981)* vol 276 p 142
[13] Glembocki O J, Shanabrook B V, Bottka N, Beard W T and Comas J 1985 *Appl. Phys. Lett.* **46** 970
[14] Berkovits V L, Gusev A O, Kochnev I V and Yavich B S 1993 *Phys. Status Solidi* **35** 564
[15] Wang G, Tronc P and Melliti R 1997 *Phys. Status Solidi* a **164** 117
[16] Aspnes D E 1980 *Handbook of Semiconductors* ed T S Moss (New York: North-Holland) p 109
[17] Aspnes D E and Studna A A 1973 *Phys. Rev.* B **7** 4605
[18] Adachi S 1985 *J. Appl. Phys.* **58** R1
[19] Voisin P, Bastard G and Voos M 1984 *Phys. Rev.* B **29** 935